A Wound-Field Three-Phase Flux-Switching Synchronous Motor with All Excitation Sources on the Stator

Ackim Zulu Barrie Mecrow Matthew Armstrong
School of Electrical, Electronic and Computer Engineering
Newcastle University, Newcastle upon Tyne NE1 7RU, United Kingdom.
Email: ackim.zulu@newcastle.ac.uk; barrie.mecrow@newcastle.ac.uk; matthew.armstrong@newcastle.ac.uk

***Abstract* -- A three-phase, segmental-rotor, flux-switching synchronous motor is presented for the first time, with both field and armature windings placed on the stator. Mutual coupling of the circuits is through segments whose motion causes switching of flux in the armature circuit. The magnetic geometry is substantially different to that of other flux-switching machines, and may offer advantages in terms of torque density and controllability. This paper describes the principles and the evaluation of a three-phase design, based on a 12-tooth stator with an 8-segment rotor before introducing a prototype machine and test results.**

***Index Terms*-- flux switching; machine windings; segmental rotor; synchronous motor; topology**

I. INTRODUCTION

There are major advantages if both the field and armature windings of a synchronous machine can be on the stator: all brushes are eliminated, whilst complete control is maintained over the field flux. This paper introduces a new form of three phase machine which has both a DC field winding and a three-phase armature winding on the stator. The operation of the motor is based on the principle of switching flux. However, the flux switching principle in this application is effected by a segmental rotor.

The flux switching motor (FSM) is a form of salient rotor reluctance machine with a novel topology, combining the principles of the inductor generator [1, 2] and the switched reluctance machine (SRM) [3]. The concept of the FSM involves changing the polarity of the flux linking the armature winding by motion of the rotor. Early principles that employed a DC field winding on the stator had a toothed rotor structure with fully-pitched windings on the stator [4]. The viability of this design was demonstrated in applications requiring high power densities and a good level of durability [5-8]. The novelty of the invention was that single-phase ac-working could be realized in the armature winding by deployment on the stator of a field winding with DC excitation and an armature winding connected to an AC supply to give the required flux orientation for rotation. Torque is developed from the changing mutual inductance of the windings. However, only single phase versions of the wound-field flux switching motor have previously been developed. Other follow-on works employing a toothed-rotor structure describe the application of permanent magnet-excitation for single phase working arrangements [9, 10] and permanent magnet or hybrid excitation for poly-phase working arrangements [11-16].

The first author is supported by the Commonwealth Scholarship Commission of the United Kingdom.

In more recent work the authors developed the use of a segmental rotor construction for SRMs [17] and two phase flux switching motors [18], which gives significant gains over other topologies. Whereas segmental rotors are used traditionally to control the saliency ratio in synchronous reluctance machines [19, 20], the primary function of the segments in this design is to provide a defined magnetic path for conveying the field flux to adjacent stator armature coils as the rotor rotates. As each coil arrangement is around a single tooth, this design gives shorter end-windings than with the toothed rotor structure which requires fully-pitched coils. There are significant gains with this arrangement as it uses less conductor materials and may improve the overall motor efficiency.

A single-phase, 8-tooth, 4-segment, field coil-excited machine developed in [18] demonstrated these attributes, and is a precursor to this work. As expected of single phase arrangements, the armature MMF induces appreciable current ripple in the DC field circuit, which can affect the control of field current.

In this work, a three-phase flux switching machine using a segmental rotor is proposed. There are clear advantages for employing arrangements with more than one phase [13], ranging from a better use of the air gap periphery and improved fault tolerance to a reduction in torque pulsations and power converter rating per phase. The paper describes the principle of operation and the design of a three-phase concept around a generic 12-tooth stator with 8 rotor segments. Predictions of performance, based on finite element simulations, and a description of a prototype machine are presented, followed by test results.

II. PRINCIPLE OF OPERATION

The term "flux switching" is coined to describe machines in which the stator tooth flux switches polarity following the motion of a salient pole rotor. All excitation sources are on the stator with the armature and field allocated to alternate stator teeth. Fig. 1 illustrates in a simplified rectilinear arrangement how a segmental rotor can achieve flux switching for a concept of four stator teeth and two rotor segments, with DC field excitation only in F1 and F2. For the two different rotor positions shown, coupling between adjacent coils on the teeth is through segments. The motion of the rotor not only varies flux in the armature teeth A1 and A2, but also changes its polarity. This results in a coil on the armature tooth experiencing a bipolar AC magnetic field,

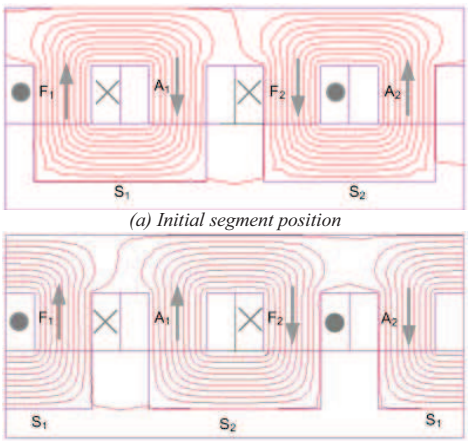

(a) Initial segment position

(b) New segment position

Fig.1 Flux distribution in stator teeth with field excitation only. F1 and F2 are field flux, A1 and A2 are armature flux, and S1 and S2 are rotor segments.

with EMF being induced.

Armature tooth flux switches polarity at two points in a cycle by two distinct presentations of the rotor segment. The first presentation for flux to switch polarity is when a segment is centered with the armature tooth, while the second presentation is when the trailing edge of one segment and the leading edge of the next segment have equal overlap over the armature tooth. This substantially contrasts with a toothed rotor or a magnetically polarized rotor, in which there is only one mechanism for switching flux. In the toothed rotor structure the mechanism may be by the transition from aligned to unaligned or vice-versa and in polarized rotors the mechanism may be by the change of the influence of an N to S pole or vice-versa.

Applying the co-energy concept [21] to the basic geometry of Fig. 1, it can be shown that the armature back-EMF e_a, and electromagnetic torque T_e, on the rotor are

$$e_a = \omega i_f \frac{dM_{fa}}{d\theta} \tag{1}$$

$$T_e = i_f i_a \frac{dM_{fa}}{d\theta} \tag{2}$$

where i_f is the field current, i_a is the armature current, θ is the rotor position, ω is the rotational speed and M_{fa} is the mutual inductance between the adjacent field and armature tooth windings. The second expression means that, as in the DC machine, torque can be directly and independently controlled using the armature and field currents.

III. The Three Phase Machine

A. Concept and Design

A three phase FSM was conceived using a stator with twelve teeth and a rotor with eight segments, S1 to S8, as shown in Fig. 2. In this design, six of the twelve stator teeth, F1 to F6, are wound as field coils and excited with DC current. These field coils produce three N poles interspersed between three S poles. The remaining six stator teeth, A1, A2, B1, B2, C1, and C2, contain six armature coils. As the rotor rotates the segments switch the armature flux so that it alternates up and down these six teeth. Each time the rotor rotates through one eighth of a revolution (one segment pitch) the flux linking the armature coils goes through a complete cycle, and so the frequency of the AC EMF induced in the

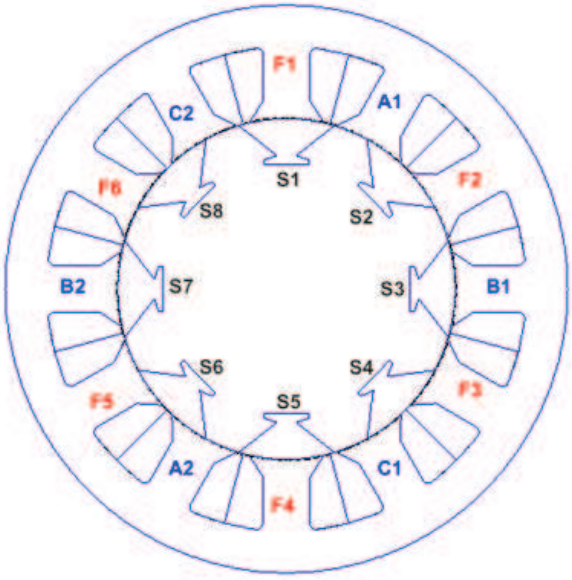

(a) structural designation

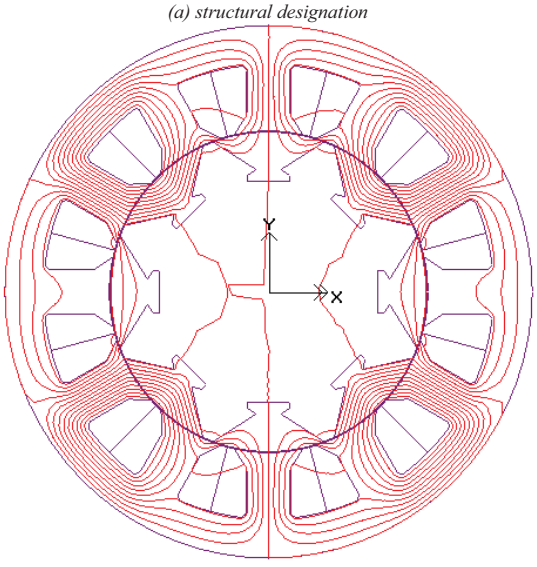

(b) flux plot at one position with field excitation only

Fig. 2. Flux distribution in stator teeth with field excitation only. F1 and F2 are field flux, A1 and A2 are armature flux, and S1 and S2 are rotor segments

stator is eight times the rotational frequency. Adjacent armature coils are displaced 60 mechanical degrees apart, corresponding to 480 electrical degrees, so that the flux and induced voltage in the stator armature coils is 120 electrical degrees apart.

The 12-8 machine of the geometry of Fig. 2 is developed. There is no cross-coupling of flux between armature phases because of the opposing polarity of the neighboring field teeth and the limit on the segment span imposed by the segment pitch in a 12-8 arrangement. This feature counts as a mark for inherent fault-tolerance [15]. As such, for optimal design, the width of each field tooth may simply be approximately the same size as the depth of the stator back-iron. However, there is a chance to use armature teeth with smaller width than field teeth under considerations of optimal magnetic circuit utilization for the 12-8 topology. This design, with the primary function of proving the concept, followed a structure of identical armature and field teeth.

An 8-segment rotor ideally gives a maximum possible segment span of 45°. To maximize armature flux linkage in this design the segment span has to be as large as possible with allowance for an acceptable segment separation that prevents flux crossing to the adjacent segments.

B. Simulations

Static 2D finite element simulations were used to determine the optimum tooth width, back-iron depth, and segment depth with a judicious use of the magnetic circuit. The segment span was optimized on the basis of maximizing the armature tooth flux linkage and parity of the alternation in the induced armature voltage. The selected sizing for an experimental machine is summarized in the dimensions shown in Table 1.

Predictions from simulations indicate that the mean torque output increases proportionally with field current and armature rms current, as shown in Fig. 3 and Fig. 4, with evidence of saturation effects at high values. There is appreciable torque ripple, but at high field and armature currents the ripple falls to a lower value, with a typical value of 40% of the instantaneous peak torque at 14 A field excitation.

Simulation results suggest that the motor has a torque capability of approximately 25 Nm motor at thermal limit. The thermal limit was experimentally determined in tests without assisted cooling and corresponds to rms currents of 14 A in the windings. In comparison with other machines of related class, on the basis of 300 W of copper loss, this design has a torque capability of about 19 Nm whereas the SRMs of similar size described in [22], from the conventional to high performance designs, have torque capabilities which range from 18.4 to 26.5 Nm.

IV. Prototype Machine

An experimental machine of the geometry of Fig. 2 was built with the specifications shown in Table 1. The stator

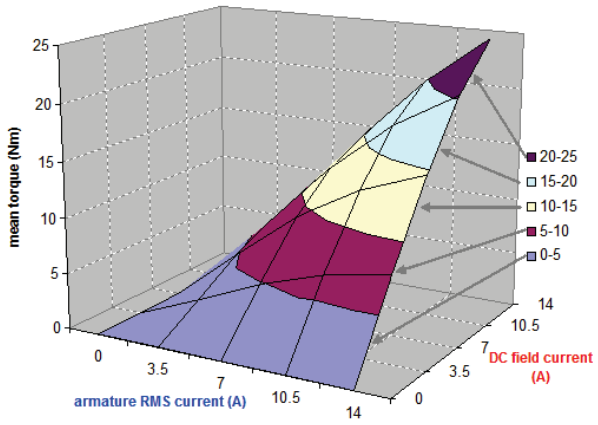

Fig. 3. Mean electromagnetic torque with varying field and armature RMS current

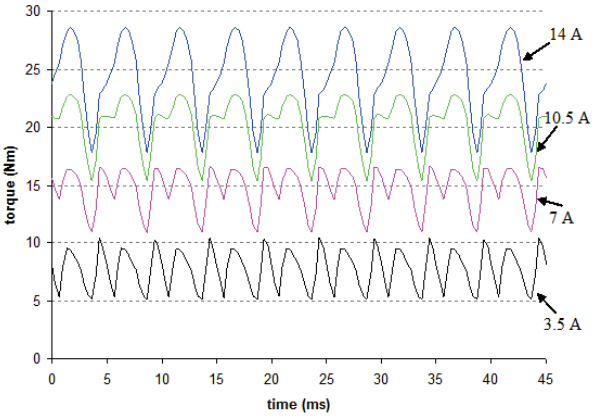

Fig. 4. Electromagnetic torque waveform at 14 A field current and varying armature RMS current

TABLE I
PRINCIPAL DIMENSIONS IN PROTOTYPE MACHINE

Stator outside diameter	150 mm
Stator back iron depth	11 mm
Stator tooth width	12.5 mm
Span of stator tooth tip	25°
Span of slot opening	5°
Rotor diameter	90.6 mm
Core axial length	150 mm
Air-gap length	0.3 mm
Segment span	41°
Segment depth (maximum)	14 mm
Number of turns per field tooth coil	44
Number of turns per armature tooth coil	44
Conductor wire diameter	1.4 mm

teeth have parallel sides with overhangs that proportionally widen towards the tips. The stator was constructed in modular fashion, using separate punching of each stator tooth in the manner of many modern servomotors [23]. This enabled the teeth to be wound before assembly of the core, giving a high slot fill-factor, about 48.2% in this case. In practice however, small gaps between the stator sections inevitably persist on assembly and tend to lower the performance by increasing the reluctance. The stator assembly was then fitted into a finned aluminum case.

The rotor laminations have semi-circular protrusions and the non-magnetic shaft of high-strength aluminum alloy is grooved with matching semi-circular indentations to enable firm press fitting on assembly. This gives a simple, but mechanically strong arrangement which may be suitable for mass production. Once pressed into the grooves, the laminations were further tightly held in place by aluminum caps bolted at both ends of the shaft. Fig. 5 shows some views of the main features of the machine.

V. Test Measurements

A set of tests were carried out on the completed motor and, where applicable, the measurements were compared with predictions from finite element simulations.

A. Static Torque

Static torque test results were measured using an in-line torque transducer with the rotor shaft locked on a rotary dividing-head, with finely defined positions over one electrical cycle. A snapshot of the instance of the three phase operating condition was represented by connecting one phase in series with the parallel combination of the other two phases to a variable DC supply. A separate variable DC supply was used for the field excitation in which the coils were all connected in series, while allowing every field coil to be in reverse polarity to the next field coil to achieve the required field flux orientation. Measured torque was compared directly with predictions made using the "Maxwell Stress" concept within the finite element simulations.

Measurements were taken at several levels of field excitation in steps of 5 A. Fig. 6 shows the results of the static torque at the rated field current of 14 A. There is a possible 7.2 % uncertainty in comparing the values of simulation and measurement results on the position scale, arising from the digitization in steps of 1^{o} (mechanical) from independent starting positions. Low values of the measurement set were also particularly susceptible to errors due to poor stability of the readings on the lower end of the range. Allowing for these errors and the assumptions of the 2D model, the measurement results agree within these reasons with the simulation results, with the worst mismatch

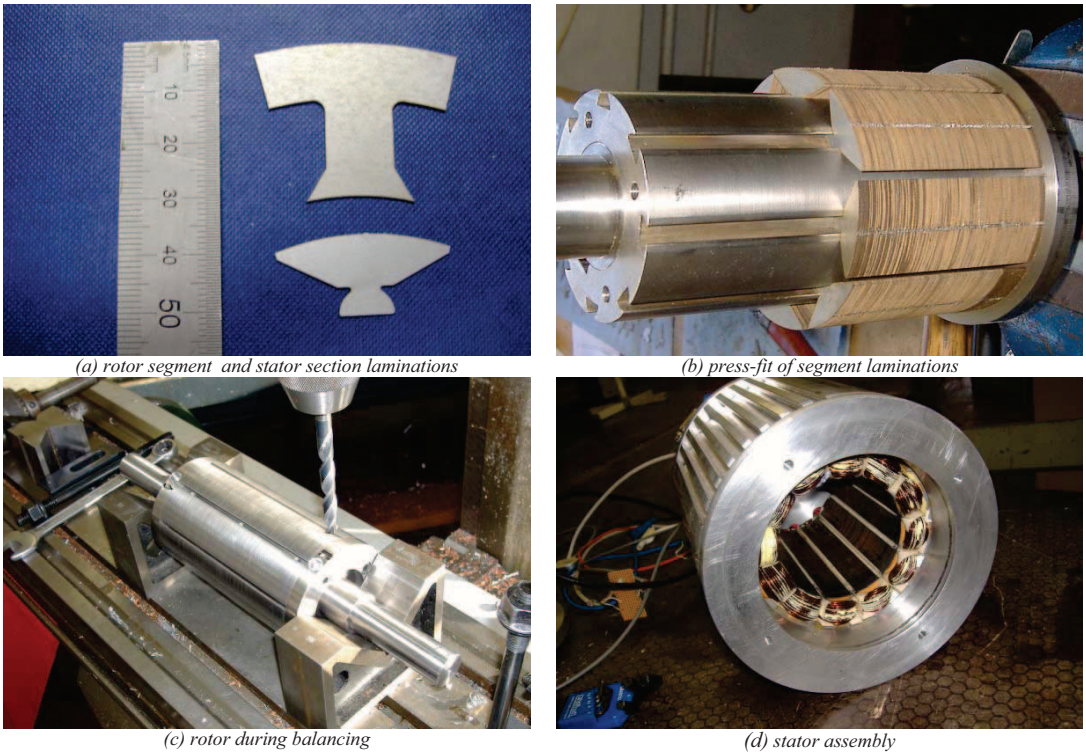

(a) rotor segment and stator section laminations

(b) press-fit of segment laminations

(c) rotor during balancing

(d) stator assembly

Fig. 5. Prototype machine components

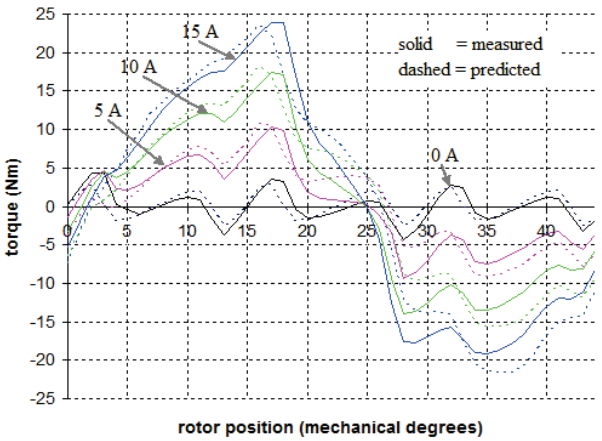

Fig. 6. Static torque at 14A field current and various armature current

in the peak values being at about 2% difference for the highest armature current used and at about 35.5% difference when no armature current is applied.

The torque rises approximately linearly to a maximum as a segment moves from the aligned position with the armature tooth and starts to fall sharply as the next segment builds overlap from the other side of the tooth. Torque changes polarity at the point where an armature tooth is overlapped in equal measure by both a receding and an approaching segment. It is also obvious to see that this is a point of torque instability with respect to position. After this position torque has changed polarity and tends to be at a constant value until there is no overlap of the first segment with the armature tooth. The torque then falls sharply but linearly as the next segment builds overlap with the armature tooth up to the alignment position, when the new cycle begins. The component of detent torque in this machine, measured when there is no current in the armature, is significant and profiles the overall torque curve with undulations when the armature is energized.

B. Running No-load Test

Another form of initial parameter measurement involved coupling the rotor of the motor under test to a brushless servomotor which acted as a prime mover. The test motor with field-only excitation was then driven by the servomotor at fixed speed. The armature EMF was observed using a high bandwidth (350 MHz) digital oscilloscope.

As in static torque, measured EMFs were compared directly against the simulations. Predicted EMF was obtained by the "flux linkage" concept from within the finite element simulations by invoking the transient analysis solver on the 2D model, over four electrical cycles. The first cycle was ignored and the results from the remaining three cycles represented the steady-state results.

Fig. 7 shows the comparison of the EMF waveforms at various field excitations at a fixed speed whilst a comparison of the measured rms EMF and the predicted fundamental rms EMF is made in Fig. 9. The simulation results show reasonable agreement with the measurement results when field excitation is less than 10 A, with the error not exceeding 5%. There was an overestimation of the predicted rms EMF values for field currents over 10 A, but this error was limited to within 10%. The error in the predicted instantaneous EMF, as compared in the positive alternation of the waveform with 14 A field excitation, was close to 18%. The waveforms of Fig. 7 indicate a significant amount of harmonics in the phase EMF. Nonetheless, the EMF waveforms generally appear more sinusoidal at higher field excitation than at lower excitation. A harmonic decomposition of the EMF on the simulation results, as shown in Fig. 8, confirm that the amount of harmonics tend to reduce as the field excitation is increased.

It is fascinating that there is no parity in the alternating parts of the EMF waveform. But this becomes clear when it is realized that the presentation of the rotor segment which produces positive alternation is different from that which produces the negative alternation. This difference results in the inequality between the percentage of the angular displacement of the rotor for changing the armature flux linkage from negative maximum to positive maximum and the angular displacement of the segment for changing the flux linkage from positive maximum to negative maximum in one electrical cycle. The points of emphasis of the inequality of two trajectories are the conditions for zero flux linkages in the armature winding. In one case this condition is reached because there is no flux passing through the tooth as a segment is fully aligned with the armature tooth. In the other case the condition is reached because of the net effect of equal and opposite flux in the tooth when the trailing edge of one segment and the leading edge of the next segment have equal overlap over the armature tooth. In the second situation, despite there being a net zero flux linkage, some parts of the tooth are experiencing considerable levels of flux density.

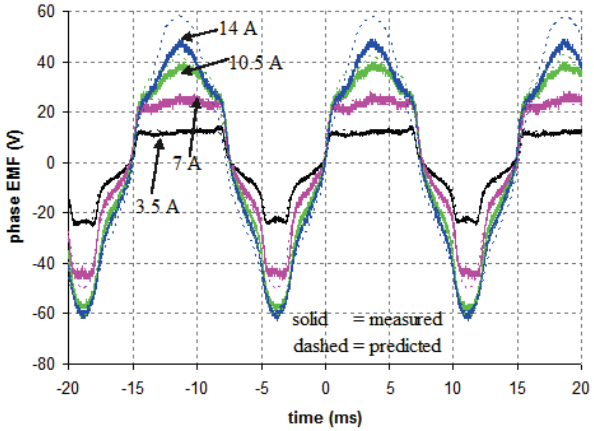

Fig. 7. Induced phase EMF waveforms at 500 rpm at various field excitation

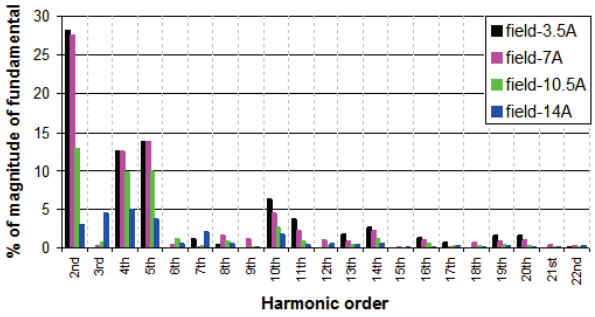

Fig. 8. Harmonic profile of predicted armature phase EMF

Despite a lack of parity in the positive and negative alternating parts of the waveforms, there is no DC component in the armature EMF at all conditions examined. The general appearance of the EMF waveform at low excitation is one with a trapezoidal shape in one alternation and a stepped trapezoidal shape in the other alternation. The linear relationship between the generated EMF and the field excitation, with indication of saturation at high excitation, is evidently apparent (Fig. 9) and so is the linear relationship between the EMF and the speed (Fig. 10).

Simulation results suggest that the terminal voltage demanded for motoring is approximately twice the armature back-EMF. Using this relationship, coupled with the form of the induced voltage-speed characteristic, it can be inferred that the motor will typically have a base speed in the range 1500-1800 rpm at 14 A field excitation if operated from a 400-V three phase drive.

C. *Load Test*

Two identical commercial three phase AC drives were used to perform load tests at a speed of 500 rev/min. The test motor was coupled to the servomotor which acted as the load machine. An absolute position encoder incorporating synchronous serial interface (SSI) standard, with 13 bit output resolution was fitted for rotor position sensing. The drive to the load machine was set up as a regenerative drive to accept electrical power from the load machine into the mains supply, whilst the drive to the test motor was set up as a motoring drive to draw electrical power from the mains supply. Fig. 11 and Fig. 12 show the setup of the testing rig.

As the drive used for testing the motor is designed for universal operation of three phase AC machines, running of the motor required adaptation to the most appropriate operating mode, 'servo mode' in this case, which for operation of traditional AC motors uses the rotor flux reference frame with stator currents placed in the quadrature axis. To use this drive, the 12-8 prototype motor was translated as an equivalent 16-pole conventional permanent-magnet synchronous motor. With closed loop speed control selected for the motor drive, the AC drive used sinusoidal current control implemented as a PWM scheme at a

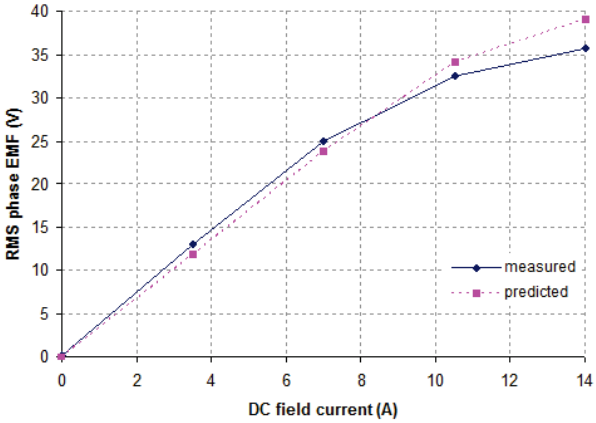

Fig. 9. Armature phase EMF versus field excitation

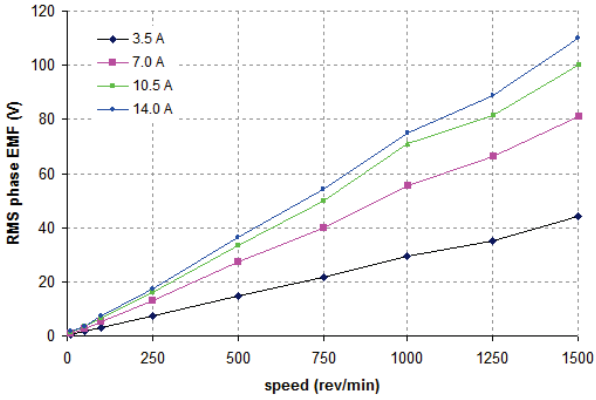

Fig. 10. Measured phase EMF versus speed for various excitations

switching frequency of 6 kHz.

The graphs in Fig. 13 verify the flexible characteristic of the torque controllable by both the field current and the armature current. The mean torque output increases proportionally with the armature current and with the field current. At high currents saturation effects come into play. Knowing that the measurement graphs are for the mechanical torque output and the simulation graphs are for the electromagnetic torque, which includes windage and friction, the differences, which range from 1.2% at low loading and 9.5% at the highest loading, are expected and also serve to underline the simulation assumptions and some mismatched measuring conditions. The measured AC armature currents used to benchmark the points for recording mechanical torque contained harmonics while the simulation values assumed pure sinusoidal armature currents, which made the actual fundamental RMS value of the measurement somewhat lower at every benchmark point. Additionally, the measured DC field current presented a ripple while the simulations used steady and constant DC values.

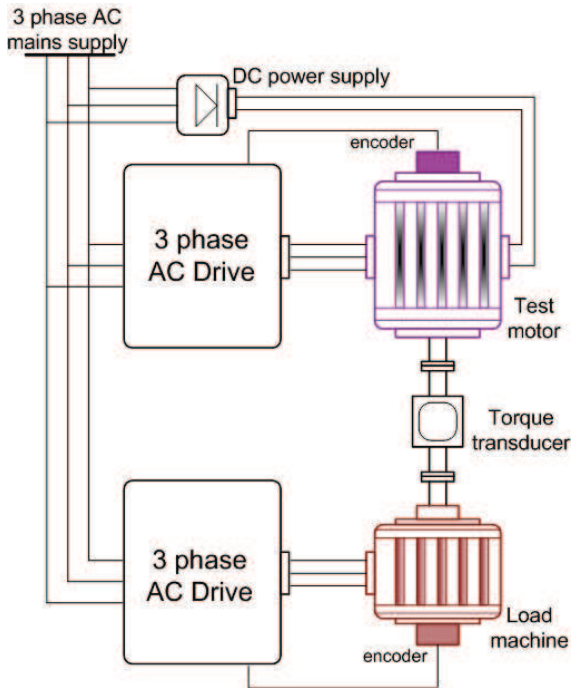

Fig. 11. Load test scheme

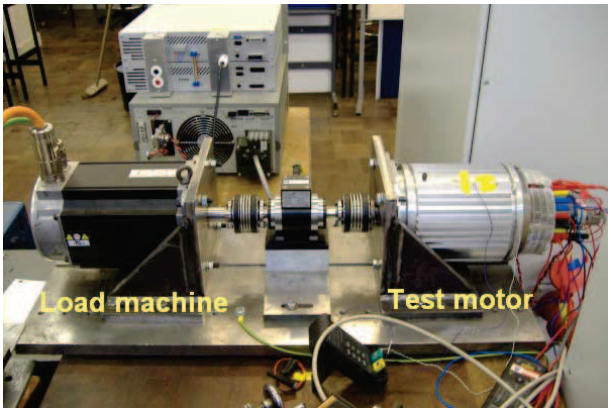

Fig. 12. Load test rig

As shown in Fig. 14, torque ripple was noticeable in the measurement results, more at low field currents and high armature currents than at other conditions. This is in contrast to the appreciable ripple in the electromagnetic torque predicted by simulations at all load conditions. It is thought that in practice and in these tests the inertia of the rotating mass has the tendency to smoothen the torque.

Current ripple in the DC field circuit was observed to be present at all load conditions, although barely perceptible at light loads. As can be seen for the situation with rated currents in Fig. 15, the ripple was at three times the electrical frequency and the peak-to-peak variation was at

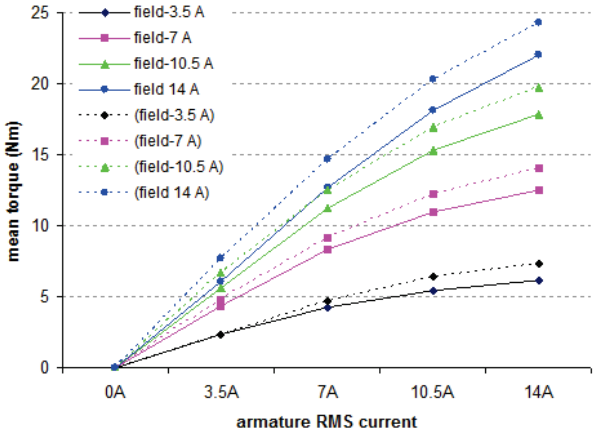

Fig. 13. Mean torque against armature current for various field excitation levels

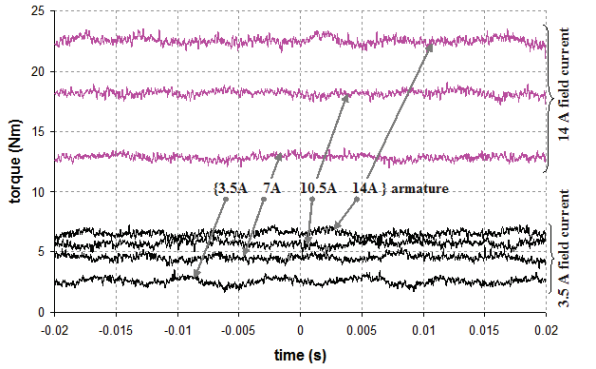

Fig. 14. Torque waveforms at various loads and excitations.

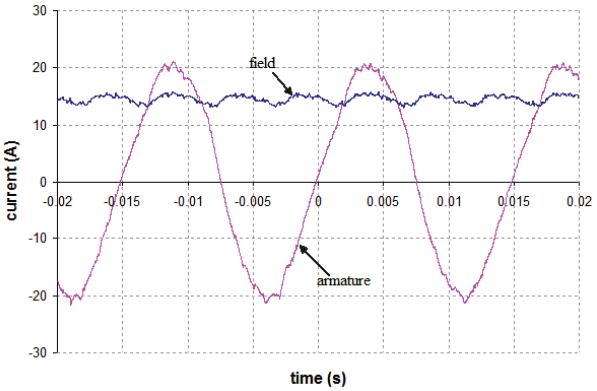

Fig. 15. Field and armature current at rated values

approximately 19% of the mean DC value. The content of current ripple observed across the range of loadings in this three phase arrangement appears to be substantially lower than that in the single-phase arrangement reported in [18], where the extent of the oscillations interfered with the

stability of current control. The postulation was that three phase configurations would eliminate current ripple in the DC field winding by coupling a resultant null effect. Evidence in this investigation shows a noticeable reduction of the ripple. This outcome is expected because the armature EMF for this design still has a substantial harmonic content.

VI. Discussion and Conclusion

This work has demonstrated the feasibility of a three-phase FSM with single-tooth windings using a segmental rotor and assignment of single-tooth armature and field windings all on the stator. The machine is capable of producing torque of comparable level with other machines of the same class, such as SRM. Control of torque by way of field current is flexible and when coupled with control by armature current gives a wide range of characteristics. However, like the SRM, the machine has appreciable torque ripple.

In general this motor topology offers some substantial appeal. The rotor can be simple, with neither magnets nor windings, which invalidates the need for brush gear. These features are a hallmark of robustness and simple construction. By comparison with permanent magnet AC machines, the field flux can be more easily controlled by simpler means which is a prospect for more efficient field weakening operation. A major drawback of this arrangement appears to be that the field winding has to use some of the slot space traditionally meant entirely for the armature winding and this may result in reduced torque density.

Upcoming work on this machine involves investigating the torque-speed characteristics with a view of demonstrating the extent of field weakening operation. Measurement of the efficiency of the motor for a direct comparison of performance with other types of machines is of interest.

Acknowledgment

The authors would like to thank C. Manning for constructing the prototype machine and the technical staff of the mechanical workshop and PEDM laboratory for help in setting up the experiments.

References

[1] J.H. Walker, 'The theory of the inductor alternator', *Journal IEE*, vol. 89, pp. 227-241, 1942.

[2] S. E. Rauch and L.J. Johnson, 'Design principles of flux-switch alternators', *Tans. AIEE*, vol. 74 pt. III, pp. 1261-1268, 1955.

[3] T.J.E. Miller, '*Switched reluctance machines and their control*', Hillsboro: Magna Physics, 1993.

[4] C. Pollock, and M. Wallace, 'The flux switching motor, a dc motor without magnets or brushes', *Proc. 1999 IEEE-Industry Applications Conf.*, vol. 3, pp. 1980-1987.

[5] H. Pollock, C. Pollock, , R.T. Walter, and B.V. Gorti, 'Low cost, high power density, flux switching machines and drives for power tools', *Proc. 2003 IEEE-Industry Applications Conf.*, pp. 1451-1457.

[6] C. Pollock, H. Pollock, and M. Brackley, 'Electronically controlled flux switching motors: a comparison with an induction motor driving an axial fan', *Proc. 2003 IEEE-Industry Applications Conf.*, pp. 2465-2470.

[7] C. Pollock, and M. Brackley, 'Comparison of the acoustic noise of a flux switching and a switched reluctance drive', *Proc. 2001 IEEE-Industry Applications Conf.*, pp. 2465-2470.

[8] C. Pollock, H. Pollock, R. Barron, J.R. Coles, D. Moule, A. Court, and R. sutton, 'Flux-switching motors for automotive applications', *IEEE Trans. Industry Applications*, vol. 42, no. 5, pp. 1177-1184, 2006.

[9] C. Cheng, C. Pollock, and H. Pollock,: 'A permanent magnet flux switching motor for low energy axial fans', *Proc. 2005 IEEE-Industry Applications Conf.*, pp. 2168-2175.

[10] Y. Chen, S. Chen, Z.Q. Zhu, D. Howe, and Y.Y. Ye, 'Starting torque of single-phase flux switching permanent magnet motors', *IEEE Trans. Magnetics*, vol. 42, no. 10, pp. 3416-3418, 2006.

[11] E. Hoang, A. H. Ben-Ahmed, and J. Lucidarme, 'Switching flux permanent magnet poly-phased synchronous machines,' *Proc. 1997 European Conf. on Power Electronics and Applications*, vol.3, pp. 903-908.

[12] E. Hoang, M. Lecrivain, and M. Gabsi, 'A new structure of a switching flux synchronous poly-phased machine with hybrid excitation,' *Proc. 2007 European Conf. on Power Electronics and Applications*, pp. 1-8.

[13] A.S. Thomas, Z.Q. Zhu, R.L. Owen, , G.W. Jewell, and D. Howe, 'Multi-phase flux switching permanent magnet machine for aerospace application', *Proc. 2008 IEEE-Industry Applications Annual Meeting*, pp. 1-8.

[14] W. Hua, M. Cheng, H. Jia, and X. Fu, 'Comparative study of flux-switching and doubly salient PM machines particlarly on torque capability', *Proc. 2008 IEEE-Industry Applications Annual Meeting*, pp. 1-8.

[15] R.L. Owen, Z.Q. Zhu, A.S. Thomas, G.W. Jewell, and D. Howe, 'Fault-tolerant flux-switching permanent magnet brushless AC machines', *Proc. 2008 IEEE-Industry Applications Annual Meeting*, pp. 1-8.

[16] Y. Pang, Z.Q. Zhu, D. Howe, S. Iwasaki, R. Deodhar, and A. Pride, 'Eddy-current loss in the frame of a flux-switching permanent magnet machine', *IEEE Trans. Magnetics*, vol. 42, no. 10, pp. 3413-3415, 2006.

[17] B.C. Mecrow, J.W. Finch, E.A. El-Kharashi, and A.G. Jack, 'Segmental rotor switched reluctance motor with single tooth windings', *Proc. IEE Electrical Power Applications*, vol. 150, no.5, pp. 591-599, 2003.

[18] B.C. Mecrow, T.J. Bedford, J.W. Bennet, and T. Celik, 'The use of segmental rotors for 2 phase flux-switching motors', *Proc. 2006 International Conf. on Electrical Machine*s, paper 608.

[19] Y. Luo, G Hwang, and K. Liu, 'Design of synchronous reluctance motor', *Proc. 1995 Electrical Electronics Insulation Conf. and Electrical Manufacturing & Coil Winding Conf.*, pp. 373-379.

[20] T. Lipo, 'Novel reluctance machine concepts for variable speed drives', *Proc. 1991 Mediterranean Electrotechnical Conf.*, pp. 34-43.

[21] A.E. Fitzgerald, C. Kingsley, S.D. Umans, *Electric machinery*, 6th ed., New York: McGraw-Hill, 2003, p. 129.

[22] B.C. Mecrow, E.A. El-Kharasi, J.W. Finch, and A.G. jack, 'Preliminary performance evaluation of switched reluctance motors with segmental rotors', *IEEE Trans. Energy Conversion*, vol. 19, no. 4, 2004.

[23] H. Akita, Y. Nakahara, N. Miyake, T. Oikawa, 'New core structure and manufacturing method for high efficiency permanent magnet motors', *Proc. 2003 IEEE-Industry Applications Conf.*, vol.1, pp. 367-372.